

Magnetic properties of moiré quantum dot arrays

Weronika Pasek,^{1,*} Michal Kupczynski,² and Pawel Potasz¹

¹*Institute of Physics, Faculty of Physics, Astronomy and Informatics,
Nicolaus Copernicus University, Grudziadzka 5, 87-100 Toruń, Poland*

²*Department of Theoretical Physics, Wrocław University of Science and Technology, 50-370 Wrocław, Poland*

(Dated: October 20, 2022)

We investigate magnetic properties of quantum dot arrays of moiré triangular superlattices. Starting from a reciprocal space model, we use projection technique to obtain maximally localized Wannier functions and determine generalized Hubbard model parameters. The many-body Hamiltonian is solved using exact diagonalization method as a function of a number of electrons in the system. Ferromagnetism is observed within a large range of filling factors for small twist angles and sufficiently strong interactions. Effective Heisenberg model with short range interactions properly determines magnetic properties at half-filling. Prospect for a magnetization controlled by applying a displacement field is presented. In a vicinity of half-filling, signatures of Nagaoka ferromagnetism in moiré materials are seen, which we demonstrate by comparing results with corresponding on-site Hubbard model.

I. INTRODUCTION

Superlattices were shown to be a promising new platform for quantum simulators [1–3]. In particular, when transition metal dichalcogenides (TMD) heterobilayer are stacked, a difference in lattice constant or a twist between the layers produces a moiré superlattice. The carriers at the top of the valence band of one of the layers experience a periodic potential formed by the other layer and many-body physics is expected to be described by a triangular lattice Hubbard model [3]. Correlated insulating state at half-filling [4–7] with antiferromagnetic Curie–Weiss behaviour [4] and a discrete series of insulating states identified as generalized Wigner crystals for partial fillings [6, 8–12] have been observed. Recently, the importance of nonlocal interaction terms due to finite high of the modulation potential strength was established [13, 14]. The role of different interaction terms in determining the ground state properties of the systems depends on a moiré potential depth, a moiré lattice constant determined by a twist angle, background dielectric screening, and a filling factor, and all of these parameters can be experimentally controlled [4, 8–10, 14, 15].

While infinite moiré systems have been intensively studied, the physics related to their finite-size fragments have been considered only at a very limited context [16]. A single moiré localization potential for small twist angles can be approximately described by a harmonic oscillator [3, 13], similarly to confining potentials in semiconductor quantum dots [17]. Quantum dots, known also as artificial atoms, are nanoscopic objects that can be considered as building blocks for artificial molecules. Different shape and size nanostructures with tunable hopping amplitude and interaction strength allow one to probe fermionic many-body physics [18–20]. Recently a few semiconductor quantum dot array patterned using the scanning tunneling microscope (STM)-based hydrogen lithography technique have been demonstrated and proposed as Fermi Hubbard model simulator [21]. The field of artificial lattices

rapidly develops and formation of artificial molecules and superlattices have been proposed and demonstrated in many semiconductor materials [22–32]. Within several advantages of solid state physics nanostructures over other platforms for quantum simulations such as ultracold atoms in optical lattices [33–36] are easy access to transport measurements, and dynamic control of the chemical potential landscape and filling factors using gates.

In this work we consider a new type of artificial molecules created from moiré superlattices and we focus on analysis of their magnetic properties. While a triangular lattice at half-filling is not expected to reveal finite spin polarization within Hubbard model, we show that moiré many-body Hamiltonian lead to a more complex magnetic phase diagram with a twist angle and interaction strength dependence. We complement our studies by analyzing exchange interaction of an effective spin model which is also valid for infinite systems. Away from half-filling we investigate a contribution to magnetization coming from itinerant electrons and discuss potential observation of Nagaoka ferromagnetism. We focus on finite size fragments of WSe_2/WS_2 heterostructure but our conclusions are valid for other heterobilayer TMDs.

II. MODEL AND METHODS

We start from a continuum model to obtain Bloch states of moiré bands of holes (see Appendix). As shown in Refs. [3, 37] the topmost moiré miniband is separated from other bands by the energy gap justifying restriction of the Hilbert space to only that band. We use projection technique to obtain corresponding exponentially localized Wannier functions [38–40]. Next, we calculate real space Coulomb matrix elements for a generalized Hubbard model. We include on-site and all direct Coulomb interactions, and non-local interaction terms, exchange and assisted hopping, because they can play a crucial role in determining many-body properties of the ground states [13]. We will consider finite size fragments of moiré superlattices with a given number of lattice sites. Hamiltonian for these moiré quantum dots arrays is written

* e-mail: weronika.pasek@doktorant.umk.pl

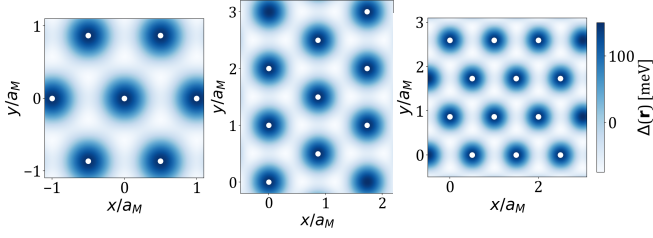


FIG. 1. The effective moiré potential forms triangular lattice with lattice constant a_M , which depends on the value of the twist angle. Three analyzed structures consists of $N = 7$ (left), $N = 9$ (middle) and $N = 12$ (right) moiré quantum dots. White dots indicate sites forming a given structure.

as

$$\begin{aligned}
 H = & - \sum_{n=1}^3 t_n \sum_{\langle i,j \rangle_n, \sigma} a_{i,\sigma}^\dagger a_{j,\sigma} + U_0 \sum_i n_{i,\downarrow} n_{i,\uparrow} \\
 & + \sum_{n=1}^3 [U_n \sum_{\langle i,j \rangle_n, \sigma, \sigma'} n_{i,\sigma} n_{j,\sigma'} - X_n \sum_{\langle i,j \rangle_n, \sigma} n_{i,\sigma} n_{j,\sigma}] \\
 & + A_n \sum_{\langle i,j \rangle_n, \sigma} (n_{i,-\sigma} + n_{j,-\sigma}) (a_{i,\sigma}^\dagger a_{j,\sigma} + H.c.),
 \end{aligned} \quad (1)$$

where $a_{i,\sigma}^\dagger$ ($a_{i,\sigma}$) is a fermionic operator, which creates (annihilates) electron with spin σ on the lattice site i , $\langle i, j \rangle_n$ depicts a pair of n -nearest neighbour sites, and $i > j$ to avoid double counting in summations. Model parameters are t_n hopping, U_0 onsite interaction, U_n direct interaction, X_n direct exchange, A_n assisted hopping, and n indicates n -th neighbors. It is expected that the effective dielectric constant ϵ determining the interaction strength (see the Appendix) lies within a range $10 < \epsilon < 20$, thus, we mainly investigate the properties of finite size systems for two values determining these limits. This estimation is based on the dielectric constant of the electrostatic environment when hexagonal boron nitride is used as the substrate, $\epsilon \approx 6$ [41] and additional screening by conducting gates and virtual transitions between the considered energy band and energetically remote moiré energy bands [13].

Calculated Hamiltonian parameters for three different twist angles are shown in Table I in the Appendix. Hamiltonian given by Eq. (1) is diagonalized in a basis of configurations corresponding to all possible distributions of particles on lattice sites. The ground state is characterized by its total spin.

III. MAGNETIC PHASE DIAGRAM FOR $N = 9$ SITES STRUCTURE

Total spin of the ground state of quantum dot array with $N = 9$ moiré lattice sites as a function filling factor $\nu = N_p/N$ (N_p is a number of particles), and twist angle is shown in Fig. 2(a) for effective dielectric constant $\epsilon = 10$ and in Fig. 2(b) for $\epsilon = 20$. The magnetic phase diagram is asymmetric with respect to half-filling, which reveal the fact that a triangular

lattice is not bipartite. For $\epsilon = 10$ finite spin polarization appears for small twist angles. With an increase of a twist angle the total spin gradually decreases for all fillings. A mechanism of vanishing spin polarization for larger twist angles is related to increase of single-particle energy levels separations, which is too large in comparison to effective exchange interaction. Near the half-filling, $\nu = 1, 1^\pm$, where 1^+ (1^-) indicates filling $\nu = 1$ plus (minus) one extra electron, the system is in the maximally spin polarized states for the twist angles $\theta < 3.5$. Away from half-filling, the magnetization is filling factor sensitive, and more stable magnetization is noticed for $\nu > 1$. The phase diagram for weaker interaction strength, $\epsilon = 20$, shown in Fig. 2(b), do not reveal spin polarization except for small twist angle region at $\nu = 1.5$. The energy level separations are here too large in comparison to Coulomb energy scales. Below we analyze in more detail a vicinity of half-filling.

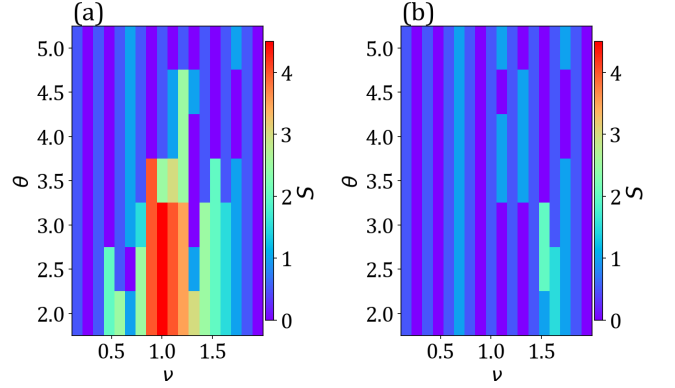


FIG. 2. The magnetic phase diagram of $N = 9$ moiré quantum dot array. Total spin of the ground state as a function of the twist angle θ and filling factor ν for fixed values of the dielectric constant (a) $\epsilon = 10$ and (b) $\epsilon = 20$.

A. Filling factor $\nu = 1$

A half-filled triangular lattice is expected to have a three sublattice antiferromagnetic order within on-site Hubbard model and a limit of strong interaction [42–45]. A finite magnetization seen in Fig. 2(a) for $\epsilon = 10$ at half-filling for small angles is related to nonzero value of direct exchange interaction due to overlap of neighboring Wannier functions, as a consequence of finite height of moiré localization potentials [13]. This direct exchange interaction has to be sufficiently large to overcome an energetic cost of occupation of higher energy states, but additionally, competes with an antiferromagnetic superexchange interaction. The physics at half-filling can be explained using effective spin model, as we will discuss below. Because

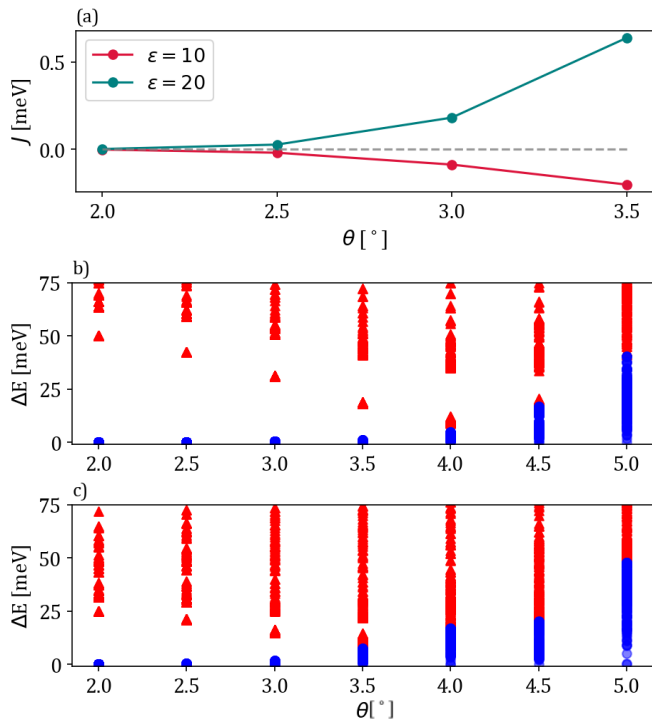


FIG. 3. (a) The effective exchange interaction J for $\epsilon = 10$ and $\epsilon = 20$ as a function of the twist angle. (b,c) Energy spectrum of many-body Hamiltonian for half-filling, $\nu = 1$, measured from the ground state $\Delta E = E_i - E_0$ for $N = 9$ moiré quantum dot array as a function of a twist angle for $\epsilon = 10$ (a) and $\epsilon = 20$ (b). Blue color marks first $2^9 = 512$ states of the lower Hubbard band. A finite energy gap between lower and upper Hubbard bands approximately indicates regimes where the description of low energy physics using effective spin model is justified.

1. Exchange J of an effective spin model

In Fig. ?? we show a comparison of effective exchange interaction J calculated given by Eq. (11) from Supplemental Material to Ref. [13]. A negative value of J indicates a ferromagnetic state and a positive one an antiferromagnetic order. A behavior of J agrees with a magnetic phase diagrams for moiré quantum dot arrays shown in Fig. 2. While according to behavior of J for $\epsilon = 10$, spin polarization should sustain for larger angles, effective spin model is not valid any longer in that regime. This is shown in Fig. 3, where we analysis the energy gap between upper and lower Hubbard bands. The lower Hubbard band consists of $2^N = 512$ spin states ($N=9$), indicated by blue circles. For small twist angles, the gap to higher energetic states from the upper Hubbard band (red triangles) is clearly visible. The gap closes when the twist angle increases, vanishing around $\theta = 4.0$ for $\epsilon = 10$, and $\theta = 3.5$ for $\epsilon = 20$. These are roughly twist angles, where a spin model approximation breaks down.

2. Charge and spin orders

We investigate charge and spin densities for half-filling for three different twist angles and $\epsilon = 20$, shown in Fig. 4. For this interaction strength the ground state has minimum total spin for all twist angles. The top row shows a charge den-

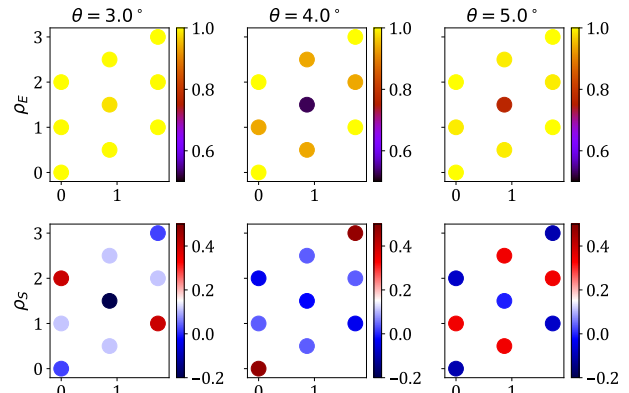


FIG. 4. The ground state charge (top row) and spin (bottom row) densities for half-filling, $\nu = 1$, for $N = 9$ moiré quantum dot array. Results obtained for three values of the twist angles θ and a dielectric constant $\epsilon = 20$.

sity distributed over quantum dots. It is quasi uniform for angle $\theta = 3.0$, as expected in a regime of spin model, and clearly nonuniform for larger twist angles. The occupation of a central quantum dot for $\theta = 4.0$ and $\theta = 5.0$ is significantly smaller comparing to eight quantum dots around, which is a consequence of direct Coulomb interaction, which is the largest for an electron in the center. One can expect that when charging the system, electrons first occupy external quantum dots and at the end the central dot. The bottom row shows corresponding spin densities. These spin densities clearly reveal two fold rotational symmetry of the quantum dot array. For angle $\theta = 3.0$, spin density in the center has negative value and the largest positive values on two quantum dots lying on shorter of two orthogonal axes determining quantum dot array symmetry. Three sublattice antiferromagnetic phase expected for an infinite triangular lattice can not be seen here because this type of quantum dot array has clearly too strong finite size effects.

3. Magnetization controlled by a displacement field

A displacement field has been used to control the moiré potential depth and induce a metal-insulator transition [15, 46]. In Fig. 5 we show that it can be used to control the magnetic properties of quantum dot arrays for half-filling. The ground state is maximally spin polarized state at the filling $\nu = 1$ and $\epsilon = 10$ without a displacement field, $V_m = 25$ meV. Applying a displacement field one can decrease the depth of a moiré localization potential V_m effectively increasing a bandwidth. The energy gap between the ground state with maximal total

spin increases its energy while the excited states with lower total spin decrease and after reaching a critical value of a displacement field the total spin is lowered.

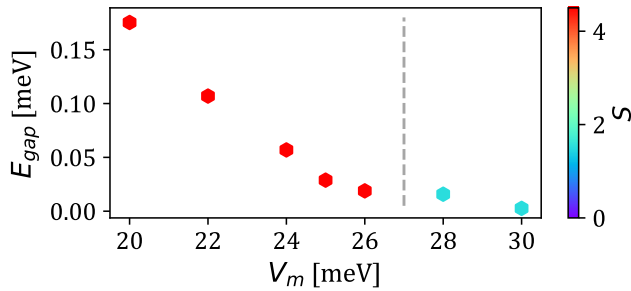


FIG. 5. The dependence of the energy gap between the ground state and the first excited state and magnetization on the depth of the effective moiré potential V_m , which can be tuned by an external electric field perpendicular to the structure. Results obtained for the half-filling $\nu = 1$, and parameters $\theta = 3.0$, $\epsilon = 10$ for $N = 9$ moiré quantum dot array.

B. Vicinity of half-filling, $\nu = 1, 1^\pm$

The ground state is maximally spin polarized in a vicinity of half-filling, $\nu = 1, 1^\pm$, as shown in Fig. 2 for $\epsilon = 10$. In Fig. 6 we analyze total spin and the energy gap between the ground state and the first excited state as a function of the interaction strength for fillings $\nu = 1, 1^\pm$ and for two twist angles, $\theta = 2.5$ and $\theta = 3.5$. The total spin is measured in relation to its maximal value at half-filling, S_{max} . A transition from the ground state with total spin $S = S_{min}$ to a state with total spin $S = S_{max}$ occurs for similar values of ϵ^{-1} for all three fillings, $\epsilon^{-1} \approx 0.1$. Above this critical value, effective exchange interaction dominates over kinetic energy. Panels (c) and (d) of Fig. 6 show evolution of the energy gaps. Above the transition to a magnetic phase the gap is the largest for filling $\nu = 1^+$ and the twist angle $\theta = 2.5$ and for half-filling $\nu = 1$ when the twist angle $\theta = 3.5$. For small twist angles, the generalized Hubbard model is closer to on-site Hubbard model, which can be seen from Ref. [13] and in particular from parameters for $\theta = 2.5$ shown in table I, where nearest neighbor hopping t_1 and onsite interaction U_0 are significantly larger comparing to other values. Because of this, we investigate Hubbard model in order to explain the origin of stability of the magnetic phase for $\nu = 1^+$ for small twist angles and, as we will show, we relate it to Nagaoka ferromagnetism.

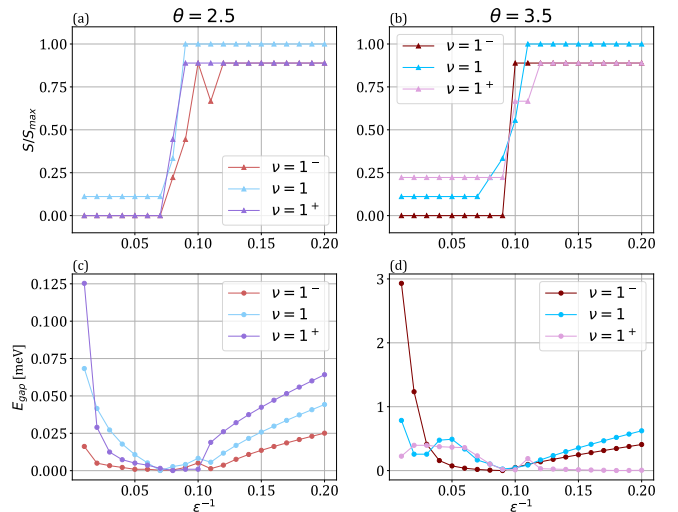


FIG. 6. The dependence of the total spin and energy gap on a dielectric constant near half-filling for two values of the twist angle, $\theta = 2.5$ (a) and (c), and $\theta = 3.5$ (b) and (d) for $N = 9$ moiré quantum dot array. A transition to a ferromagnetic phase is seen around $\epsilon \approx 10$ for both angles.

C. Hubbard model and Nagaoka ferromagnetism for filling factor $\nu = 1^+$

We consider on-site Hubbard model [47] given by the Hamiltonian

$$H = t_1 \sum_{\langle i,j \rangle, \sigma} a_{i,\sigma}^\dagger a_{j,\sigma} + U_0 \sum_i n_{i,\downarrow} n_{i,\uparrow} \quad (2)$$

with parameters U_0 and t_1 taken from table I for twist angle $\theta = 2.5$. Fig. 7 shows total spin of the ground state in panel (a) and the energy gap between the ground state and first excited state in panel (c) as a function of the filling factor and interaction strength $\epsilon = 10$. There is a finite range of fillings $1 < \nu < 1.5$ with maximal possible spin polarization. Values of energy gaps suggest stronger stability of magnetic phases farther from half-filling.

When one electron or one hole is added to the half-filled system, $\nu = 1$, a transition to maximally spin polarized state is expected within Hubbard model in a limit of infinite U_0 interaction due to Nagaoka ferromagnetism [48]. Whether on which side of the half-filling it occurs, for $\nu = 1^-$ or $\nu = 1^+$, depends on a lattice type. For a triangular lattice, Nagaoka ferromagnetism is expected for Hubbard model for $\nu = 1^+$ because a ferromagnetic state was shown to be unstable for $\nu = 1^-$ with respect to a Gutzwiller single spin flip [49, 50]. Indeed, we see it in a Hubbard model results, and it is the reason of increased energy gap in moiré quantum dot arrays for this filling shown in Fig. 6. Panel (b) and panel (d) of Fig. 7 analyze vicinity of half-filling, $\nu = 1, 1^\pm$, when interaction strength is varied, the total spin and the energy gap, respectively. A transition to the maximal spin polarized ground state occurs only for $\nu = 1^+$ for $\epsilon^{-1} \approx 0.05$. The energy gap increases with increase of interactions strength but saturates at

a constant value already around $\varepsilon^{-1} \approx 0.15$

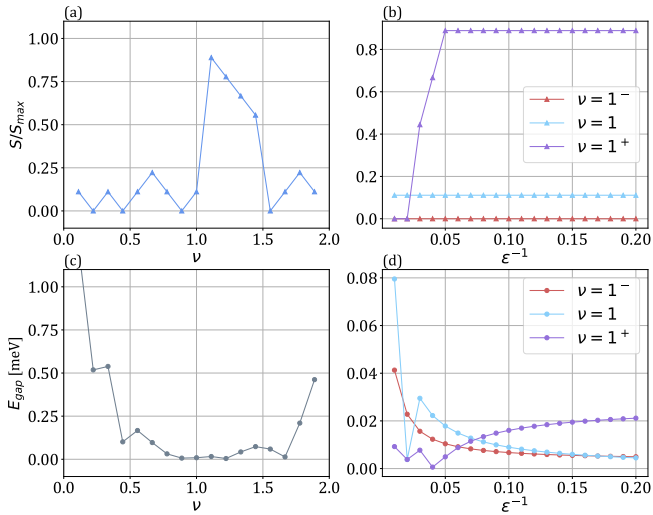


FIG. 7. Results obtained for the Hubbard model, Eq. (2) for $N = 9$ structure. (a) Total spin of the ground state and (c) the energy gap as functions of the filling factor for $\varepsilon = 10$ and $\theta = 2.5$. (b) Total spin and (d) the energy gap for fillings $\nu = 1^-, 1, 1^+$ and $\theta = 2.5$ as a function of an interaction strength.

IV. SHAPE DEPENDENT MAGNETIZATION IN MOIRÉ QUANTUM DOT ARRAYS

We consider structures consisting of $N = 7$, $N = 9$, and $N = 12$ quantum dots. Fig. 8 shows total spin of the ground state as a function of filling factor ν for systems with two twist angles, $\theta = 2.5$ and $\theta = 3.5$. Full spin polarization is seen at half filling for $N = 7$ and $N = 9$ structures for twist angle $\theta = 2.5$, and only partial spin polarization for $N = 12$. Magnetization seems to disappear at half-filling when a system size increases but this should be the effect of a particular geometry of the largest structure we consider with $N = 12$ quantum dots because from effective exchange interaction J of a spin model one predicts a ferromagnetic state for $\varepsilon = 10$ in a limit of an infinite system, Fig. ??(a). In general, spin polarization is filling factor dependent for all structures, and a tendency to spin polarization is stronger for fillings $\nu > 1$. This is in particular evident around $\nu = 1.5$, where all structures reveal finite magnetization. We relate it to van Hove singularity in a density of states of a triangular lattice [3].

V. CONCLUSIONS

We investigated magnetic properties of various moiré quantum dot arrays and concentrate on detail analysis of a structure with $N = 9$ sites. We show that the structures reveal finite spin polarization for small twist angles and sufficiently strong interaction strength. The origin of magnetization is two-fold.

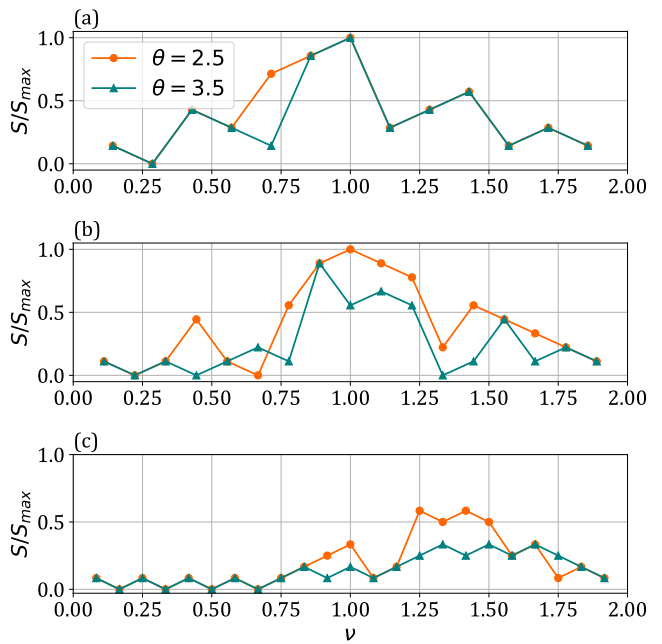


FIG. 8. The comparison of magnetic phase diagrams for three moiré quantum dot arrays with $N = 7$ (top row), $N = 9$ (middle row) and $N = 12$ (bottom row). Value of the dielectric constant is fixed to $\varepsilon = 10$.

The main factor is direct exchange interaction due to nonzero overlap of Wannier functions from neighboring moiré lattice sites. This leads to maximal spin polarization at half-filling that otherwise would not be expected on a triangular lattice. Additionally, there is a contribution to magnetization due to mechanism proposed by Nagaoka as the effect of constructive interference between different paths of electrons moving in a spin polarized background. This can lead to more stable magnetization away from half-filling in comparison to the half-filling case. Nagaoka ferromagnetism is expected to vanish in a thermodynamic limit because the energy gap between the spin polarized ground state and the excited states vanish. In moiré quantum dot arrays this energy gap should still be finite, and, as we show, is filling factor dependent. Whether magnetization at half-filling or away from it is more stable depends on which of these two factors dominates. Appropriate choice of materials forming TMD heterostructure, size and shape of moiré quantum dot arrays, and the twist angle can allow to design magnetic nanostructures with a filling factor dependent magnetization.

ACKNOWLEDGMENTS

The authors acknowledge helpful interactions with M. Zielinski. PP acknowledges support from the Polish National Science Centre based on Decision No. 2021/41/B/ST3/03322. MK acknowledges support from the Polish National Science Centre based on Decision No. 2019/33/N/ST3/03137. Cal-

culations were performed using the Wrocław Center for Networking and Supercomputing WCSS.

-
- [1] E. Y. Andrei, D. K. Efetov, P. Jarillo-Herrero, A. H. MacDonald, K. F. Mak, T. Senthil, E. Tutuc, A. Yazdani, and A. F. Young, The marvels of moiré materials, *Nature Reviews Materials* **6**, 201 (2021).
- [2] D. M. Kennes, M. Claassen, L. Xian, A. Georges, A. J. Millis, J. Hone, C. R. Dean, D. N. Basov, A. N. Pasupathy, and A. Rubio, Moiré heterostructures as a condensed-matter quantum simulator, *Nature Physics* **17**, 155 (2021).
- [3] F. Wu, T. Lovorn, E. Tutuc, and A. H. MacDonald, Hubbard model physics in transition metal dichalcogenide moiré bands, *Phys. Rev. Lett.* **121**, 026402 (2018).
- [4] Y. Tang, L. Li, T. Li, Y. Xu, S. Liu, K. Barmak, K. Watanabe, T. Taniguchi, A. H. MacDonald, J. Shan, and K. F. Mak, Simulation of hubbard model physics in wse2/ws2 moiré superlattices, *Nature* **579**, 353 (2020).
- [5] Y. Shimazaki, I. Schwartz, K. Watanabe, T. Taniguchi, M. Kroner, and A. Imamoğlu, Strongly correlated electrons and hybrid excitons in a moiré heterostructure, *Nature* **580**, 472 (2020).
- [6] E. C. Regan, D. Wang, C. Jin, M. I. Bakti Utama, B. Gao, X. Wei, S. Zhao, W. Zhao, Z. Zhang, K. Yumigeta, M. Blei, J. D. Carlström, K. Watanabe, T. Taniguchi, S. Tongay, M. Crommie, A. Zettl, and F. Wang, Mott and generalized wigner crystal states in wse2/ws2 moiré superlattices, *Nature* **579**, 359 (2020).
- [7] L. Wang, E.-M. Shih, A. Ghiotto, L. Xian, D. A. Rhodes, C. Tan, M. Claassen, D. M. Kennes, Y. Bai, B. Kim, K. Watanabe, T. Taniguchi, X. Zhu, J. Hone, A. Rubio, A. N. Pasupathy, and C. R. Dean, Correlated electronic phases in twisted bilayer transition metal dichalcogenides, *Nature Materials* **19**, 861 (2020).
- [8] Y. Xu, S. Liu, D. A. Rhodes, K. Watanabe, T. Taniguchi, J. Hone, V. Elser, K. F. Mak, and J. Shan, Correlated insulating states at fractional fillings of moiré superlattices, *Nature* **587**, 214 (2020).
- [9] X. Huang, T. Wang, S. Miao, C. Wang, Z. Li, Z. Lian, T. Taniguchi, K. Watanabe, S. Okamoto, D. Xiao, S.-F. Shi, and Y.-T. Cui, Correlated insulating states at fractional fillings of the ws2/wse2 moiré lattice, *Nature Physics* [10.1038/s41567-021-01171-w](https://doi.org/10.1038/s41567-021-01171-w) (2021).
- [10] C. Jin, Z. Tao, T. Li, Y. Xu, Y. Tang, J. Zhu, S. Liu, K. Watanabe, T. Taniguchi, J. C. Hone, L. Fu, J. Shan, and K. F. Mak, Stripe phases in wse2/ws2 moiré superlattices, *Nature Materials* [10.1038/s41563-021-00959-8](https://doi.org/10.1038/s41563-021-00959-8) (2021).
- [11] Y. Tang, J. Gu, S. Liu, K. Watanabe, T. Taniguchi, J. C. Hone, K. F. Mak, and J. Shan, Dielectric catastrophe at the mott and wigner transitions in a moiré superlattice (2022), [arXiv:2201.12510 \[cond-mat.mtrl-sci\]](https://arxiv.org/abs/2201.12510).
- [12] H. Li, S. Li, E. C. Regan, D. Wang, W. Zhao, S. Kahn, K. Yumigeta, M. Blei, T. Taniguchi, K. Watanabe, S. Tongay, A. Zettl, M. F. Crommie, and F. Wang, Imaging two-dimensional generalized wigner crystals, *Nature* **597**, 650 (2021).
- [13] N. Morales-Durán, N. C. Hu, P. Potasz, and A. H. MacDonald, Nonlocal interactions in moiré hubbard systems, *Phys. Rev. Lett.* **128**, 217202 (2022).
- [14] Y. Tang, K. Su, L. Li, Y. Xu, S. Liu, K. Watanabe, T. Taniguchi, J. Hone, C.-M. Jian, C. Xu, K. F. Mak, and J. Shan, *Frustrated magnetic interactions in a wigner-mott insulator* (2022).
- [15] T. Li, S. Jiang, L. Li, Y. Zhang, K. Kang, J. Zhu, K. Watanabe, T. Taniguchi, D. Chowdhury, L. Fu, J. Shan, and K. F. Mak, Continuous mott transition in semiconductor moiré superlattices, *Nature* **597**, 350 (2021).
- [16] Y. Zeng and A. H. MacDonald, The strong modulation limit of excitons and trions in moiré materials, (2021), [arXiv:2110.00106v1 \[cond-mat.str-el\]](https://arxiv.org/abs/2110.00106v1).
- [17] L. Jacak, P. Hawrylak, and A. Wojs, Quantum dots, Springer Berlin Heidelberg doi.org/10.1007/978-3-642-72002-4 (1997).
- [18] J. Salfi, J. Mol, R. Rahman, G. Klimeck, M. Simmons, L. Hollenberg, and S. Rogge, Quantum simulation of the hubbard model with dopant atoms in silicon, *Nature communications* **7**, 1 (2016).
- [19] T. Hensgens, T. Fujita, L. Janssen, X. Li, C. Van Diepen, C. Reichl, W. Wegscheider, S. Das Sarma, and L. M. Vandersypen, Quantum simulation of a fermi–hubbard model using a semiconductor quantum dot array, *Nature* **548**, 70 (2017).
- [20] J. P. Dehollain, U. Mukhopadhyay, V. P. Michal, Y. Wang, B. Wunsch, C. Reichl, W. Wegscheider, M. S. Rudner, E. Demler, and L. M. Vandersypen, Nagaoka ferromagnetism observed in a quantum dot plaquette, *Nature* **579**, 528 (2020).
- [21] W. Xiqiao, K. Ehsan, F. Fan, W. Jonathan, N. Pradeep, K. Ranjit, R. Albert, F. B. Garnett, and S. Richard, Quantum simulation of an extended fermi-hubbard model using a 2d lattice of dopant based quantum dots, (2021), [arXiv:2110.08982 \[cond-mat.str-el\]](https://arxiv.org/abs/2110.08982).
- [22] A. Singha, M. Gibertini, B. Karmakar, S. Yuan, M. Polini, G. Vignale, M. Katsnelson, A. Pinczuk, L. Pfeiffer, K. West, *et al.*, Two-dimensional mott-hubbard electrons in an artificial honeycomb lattice, *Science* **332**, 1176 (2011).
- [23] K. K. Gomes, W. Mar, W. Ko, F. Guinea, and H. C. Manoharan, Designer dirac fermions and topological phases in molecular graphene, *Nature* **483**, 306 (2012).
- [24] T. Uehlinger, G. Jotzu, M. Messer, D. Greif, W. Hofstetter, U. Bissbort, and T. Esslinger, Artificial graphene with tunable interactions, *Phys. Rev. Lett.* **111**, 185307 (2013).
- [25] S. Wang, L. Z. Tan, W. Wang, S. G. Louie, and N. Lin, Manipulation and characterization of aperiodical graphene structures created in a two-dimensional electron gas, *Phys. Rev. Lett.* **113**, 196803 (2014).
- [26] R. Drost, T. Ojanen, A. Harju, and P. Liljeroth, Topological states in engineered atomic lattices, *Nature Physics* **13**, 668 (2017).
- [27] M. R. Slot, T. S. Gardenier, P. H. Jacobse, G. C. Van Miert, S. N. Kempkes, S. J. Zevenhuizen, C. M. Smith, D. Vanmaekelbergh, and I. Swart, Experimental realization and characterization of an electronic lieb lattice, *Nature Physics* **13**, 672 (2017).
- [28] C. Forsythe, X. Zhou, K. Watanabe, T. Taniguchi, A. Pasupathy, P. Moon, M. Koshino, P. Kim, and C. R. Dean, Band structure engineering of 2d materials using patterned dielectric superlattices, *Nature nanotechnology* **13**, 566 (2018).
- [29] C.-H. Park and S. G. Louie, Making massless dirac fermions from a patterned two-dimensional electron gas, *Nano letters* **9**, 1793 (2009).
- [30] S. Wang, D. Scarabelli, L. Du, Y. Y. Kuznetsova, L. N. Pfeiffer, K. W. West, G. C. Gardner, M. J. Manfra, V. Pellegrini, S. J. Wind, *et al.*, Observation of dirac bands in artificial graphene in small-period nanopatterned gaas quantum wells, *Nature nan-*

- otechnology **13**, 29 (2018).
- [31] A. Biborski, M. P. Nowak, and M. Zegrodnik, Correlation-induced d -wave pairing in a quantum dot square lattice, *Phys. Rev. B* **104**, 245430 (2021).
- [32] Y. Saleem, A. Dusko, M. Cygorek, M. Korkusinski, and P. Hawrylak, Quantum simulator of extended bipartite hubbard model with broken sublattice symmetry: Magnetism, correlations, and phase transitions, *Phys. Rev. B* **105**, 205105 (2022).
- [33] I. Bloch, Ultracold quantum gases in optical lattices, *Nature physics* **1**, 23 (2005).
- [34] L. Tarruell and L. Sanchez-Palencia, Quantum simulation of the hubbard model with ultracold fermions in optical lattices, *Comptes Rendus Physique* **19**, 365 (2018), quantum simulation / Simulation quantique.
- [35] A. Mazurenko, C. S. Chiu, G. Ji, M. F. Parsons, M. Kanász-Nagy, R. Schmidt, F. Grusdt, E. Demler, D. Greif, and M. Greiner, A cold-atom fermi–hubbard antiferromagnet, *Nature* **545**, 462 (2017).
- [36] C. Gross and I. Bloch, Quantum simulations with ultracold atoms in optical lattices, *Science* **357**, 995 (2017).
- [37] N. Morales-Durán, A. H. MacDonald, and P. Potasz, Metal-insulator transition in transition metal dichalcogenide heterobilayer moiré superlattices, *Phys. Rev. B* **103**, L241110 (2021).
- [38] J. D. Cloizeaux, Energy bands and projection operators in a crystal: Analytic and asymptotic properties, *Phys. Rev.* **135**, A685 (1964).
- [39] J. D. Cloizeaux, Analytical properties of n -dimensional energy bands and wannier functions, *Phys. Rev.* **135**, A698 (1964).
- [40] N. Marzari and D. Vanderbilt, Maximally localized generalized wannier functions for composite energy bands, *Phys. Rev. B* **56**, 12847 (1997).
- [41] A. V. Stier, N. P. Wilson, G. Clark, X. Xu, and S. A. Crooker, Probing the influence of dielectric environment on excitons in monolayer wse2: insight from high magnetic fields, *Nano letters* **16**, 7054 (2016).
- [42] T. Ohashi, T. Momoi, H. Tsunetsugu, and N. Kawakami, Finite temperature mott transition in hubbard model on anisotropic triangular lattice, *Phys. Rev. Lett.* **100**, 076402 (2008).
- [43] T. Yoshioka, A. Koga, and N. Kawakami, Quantum phase transitions in the hubbard model on a triangular lattice, *Phys. Rev. Lett.* **103**, 036401 (2009).
- [44] G. Rohringer, H. Hafermann, A. Toschi, A. A. Katanin, A. E. Antipov, M. I. Katsnelson, A. I. Lichtenstein, A. N. Rubtsov, and K. Held, Diagrammatic routes to nonlocal correlations beyond dynamical mean field theory, *Rev. Mod. Phys.* **90**, 025003 (2018).
- [45] T. Cookmeyer, J. Motruk, and J. E. Moore, Four-spin terms and the origin of the chiral spin liquid in mott insulators on the triangular lattice, *Phys. Rev. Lett.* **127**, 087201 (2021).
- [46] A. Ghiotto, E.-M. Shih, G. S. S. G. Pereira, D. A. Rhodes, B. Kim, J. Zang, A. J. Millis, K. Watanabe, T. Taniguchi, J. C. Hone, L. Wang, C. R. Dean, and A. N. Pasupathy, Quantum criticality in twisted transition metal dichalcogenides, *Nature* **597**, 345 (2021).
- [47] J. Hubbard, Electron correlations in narrow energy bands, *Proceedings of the Royal Society of London. Series A, Mathematical and Physical Sciences* **276**, 238 (1963).
- [48] Y. Nagaoka, Ferromagnetism in a narrow, almost half-filled s band, *Physical Review* **147**, 392 (1966).
- [49] T. Hanisch, B. Kleine, A. Ritzl, and E. Müller-Hartmann, Ferromagnetism in the hubbard model: instability of the nagaoka state on the triangular, honeycomb and kagome lattices, *Annalen der Physik* **507**, 303 (1995).
- [50] T. Hanisch, G. S. Uhrig, and E. Müller-Hartmann, Lattice dependence of saturated ferromagnetism in the hubbard model, *Physical Review B* **56**, 13960 (1997).

APPENDIX

Continuum model and Wannier functions from projection technique

The valley-projected continuum Hamiltonian for TMD moiré heterobilayers is written as [3]

$$H = -\frac{\hbar^2}{2m^*} \mathbf{k}^2 + \Delta(\mathbf{r}), \quad (3)$$

where $m^* = 0.35m_0$ [3, 13] is the effective mass of charge carriers in the valence band of the active layer and a modulation potential $\Delta(\mathbf{r}) = 2V_m \sum_{j=1,3,5} \cos(\mathbf{b}_j \cdot \mathbf{r} + \phi)$ with $\mathbf{b}_j = 4\pi/\sqrt{3}a_M (\cos(\pi j/3), \sin(\pi j/3))$, belonging to the first shell of reciprocal lattice vectors with $V_m = 25$ meV and $\phi = -94^\circ$, which determine the strength of the potential and the location of its minima, respectively. The Hamiltonian given by Eq. (3) is diagonalized in a plane wave basis giving energies E_n and eignestates $|\Psi_n(\mathbf{k})\rangle$. Bloch $|\Psi(\mathbf{k})\rangle$ of the topmost valence band (we omit the band index) are

$$|\Psi(\mathbf{k})\rangle = \sum_{\mathbf{G}} z_{\mathbf{k}+\mathbf{G}} e^{i(\mathbf{k}+\mathbf{G})\mathbf{r}}, \quad (4)$$

where $z_{\mathbf{k}+\mathbf{G}}$ are expansion coefficients.

We use a projection technique [38–40] to obtain Wannier functions of holes localized on moiré superlattice sites. We project trial wavefunction $|t_i(\mathbf{r})\rangle$, with corresponding Fourier transform $|t_i(\mathbf{k})\rangle$ onto Bloch function $|\Psi(\mathbf{k})\rangle$ of topmost valence band of moiré band structure. One has

$$|\gamma_i(\mathbf{k})\rangle = P(\mathbf{k})|t_i(\mathbf{k})\rangle = |\Psi(\mathbf{k})\rangle \langle \Psi(\mathbf{k}) | t_i(\mathbf{k}) \rangle$$

with overlap

$$S = \langle t_i(\mathbf{k}) | P(\mathbf{k}) | t_i(\mathbf{k}) \rangle = \langle t_i(\mathbf{k}) | \Psi(\mathbf{k}) \rangle \langle \Psi(\mathbf{k}) | t_i(\mathbf{k}) \rangle = |\langle \Psi(\mathbf{k}) | t_i(\mathbf{k}) \rangle|^2$$

and orthogonal new quasi-Bloch states are

$$|\tilde{\Psi}(\mathbf{k})\rangle = (S^{-1/2})|\gamma(\mathbf{k})\rangle = |\Psi(\mathbf{k})\rangle \frac{\langle \Psi(\mathbf{k})|t(\mathbf{k})\rangle}{|\langle \Psi(\mathbf{k})|t(\mathbf{k})\rangle|} = |\Psi(\mathbf{k})\rangle e^{-i\theta_t(\mathbf{k})}, \quad (5)$$

which means that the projection technique is equivalent to appropriate $\theta_t(\mathbf{k})$ phase fixing of Bloch states in order to have corresponding exponentially localized Wannier functions on lattice site i . We choose trial state $|t_i\rangle$ as delta function (Gaussian like trial wavefunction gives similar results) localized at a given site of a crystal lattice,

$$|t_i(\mathbf{r})\rangle = \delta(\mathbf{r} - \boldsymbol{\tau}_i)$$

where $\boldsymbol{\tau}_i$ determines a position of a lattice site. Fourier transform of it is

$$|t_i(\mathbf{k})\rangle = \frac{1}{\sqrt{N_G}} \sum_{\mathbf{G}} e^{i(\mathbf{k}+\mathbf{G})(\mathbf{r}-\boldsymbol{\tau}_i)}$$

where N_G is a number of reciprocal basis vectors \mathbf{G} . One has an overlap with Bloch state

$$\langle \Psi(\mathbf{k})|t(\mathbf{k})\rangle = \frac{1}{\sqrt{N_G}} \sum_{\mathbf{G}, \mathbf{G}'} z_{\mathbf{k}+\mathbf{G}}^* \int d\mathbf{r} e^{-i(\mathbf{k}+\mathbf{G}')\mathbf{r}} e^{i(\mathbf{k}+\mathbf{G})(\mathbf{r}-\boldsymbol{\tau}_i)} = \frac{V_{cell}}{\sqrt{N_G}} \sum_{\mathbf{G}} z_{\mathbf{k}+\mathbf{G}}^* e^{-i(\mathbf{k}+\mathbf{G})\boldsymbol{\tau}_i},$$

where V_{cell} is the unit cell volume. After above procedure of fixing the phase of the topmost valence band, eigenstates corresponding localized Wannier functions can be obtained

$$|\mathbf{R}\rangle = \frac{1}{\sqrt{N}} \sum_{\mathbf{k}} e^{-i\mathbf{k}\cdot\mathbf{R}} |\tilde{\Psi}(\mathbf{k})\rangle, \quad (6)$$

where \mathbf{R} are Wannier center positions on a moiré triangular lattice and N is the number of moiré unit cells. Four-center real space Coulomb matrix elements are

$$\langle \mathbf{R}_i, \mathbf{R}_j | V | \mathbf{R}_k, \mathbf{R}_l \rangle = \frac{1}{N^2} \sum_{\substack{\mathbf{k}_i, \mathbf{k}_j \\ \mathbf{k}_k, \mathbf{k}_l}} e^{i(\mathbf{k}_i \cdot \mathbf{R}_i + \mathbf{k}_j \cdot \mathbf{R}_j - \mathbf{k}_k \cdot \mathbf{R}_k - \mathbf{k}_l \cdot \mathbf{R}_l)} \langle \tilde{\Psi}(\mathbf{k}_i), \tilde{\Psi}(\mathbf{k}_j) | V | \tilde{\Psi}(\mathbf{k}_k), \tilde{\Psi}(\mathbf{k}_l) \rangle, \quad (7)$$

with $V = \frac{e^2}{4\pi\epsilon_0\epsilon|\mathbf{r}_1-\mathbf{r}_2|}$, with e as electric charge and ϵ_0 is the vacuum permittivity, \mathbf{r}_i is position of i -th particle, and two-center integrals are: U_0 ($i = j = k = l$), U_1 ($i = l, j = k$ and i, j are nearest neighbors), X_1 ($i = k, j = l$ and i, j are nearest neighbors), A ($i = j = k$, and i, l are nearest neighbors). We also take $U_n = U_1/r_n$, where r_n is a distance to n -th nearest neighbors, assuming $r_1 = 1$ for nearest neighbors. We perform calculations of Coulomb elements in a reciprocal space using Bloch state defined by Eq. 5. Tight-binding hopping integrals are given by

$$t_n = \frac{1}{N} \sum_{\mathbf{k}} e^{-i\mathbf{k}(\mathbf{R}_i - \mathbf{R}_j)} E_{\mathbf{k}}, \quad (8)$$

where $n = 1$ for (i, j) nearest neighbors and $n = 2$ for (i, j) next nearest neighbors, and $n = 3$ for (i, j) next-next nearest neighbors. In order to confirm validity of our real-space parameters we have compared exact diagonalization results starting from a continuum model and with real space parameters obtaining satisfactory agreement for a periodic system with $N = 9$ unit cells (3×3 momentum space mesh) and $N_{el} = 9$ particles. Generalized Hubbard model parameters are presented in table I.

θ	t_1	t_2	t_3	U_0	U_1	X_1	A_1
2.5	0.653	-0.024	-0.0147	1086.925	158.632	0.308	-3.301
3.5	3.341	-0.389	-0.217	1143.612	229.822	4.057	-4.135
5.0	10.351	-2.066	-1.032	1232.254	336.887	17.387	10.006

TABLE I. Generalized Hubbard model parameters for different twist angles θ . All parameters are in meV and interaction parameters for $\epsilon = 1$.